



This is the accepted manuscript made available via CHORUS. The article has been published as:

## Local and Nonlocal Transport Spectroscopy in Planar Josephson Junctions

A. Banerjee, O. Lesser, M. A. Rahman, C. Thomas, T. Wang, M. J. Manfra, E. Berg, Y. Oreg, Ady Stern, and C. M. Marcus

Phys. Rev. Lett. **130**, 096202 — Published 28 February 2023

DOI: [10.1103/PhysRevLett.130.096202](https://doi.org/10.1103/PhysRevLett.130.096202)

# Local and Nonlocal Transport Spectroscopy in Planar Josephson Junctions

A. Banerjee,<sup>1</sup> O. Lesser,<sup>2</sup> M. A. Rahman,<sup>1</sup> C. Thomas,<sup>3</sup> T. Wang,<sup>3</sup>  
M. J. Manfra,<sup>3,4</sup> E. Berg,<sup>2</sup> Y. Oreg,<sup>2</sup> Ady Stern,<sup>2</sup> and C. M. Marcus<sup>1</sup>

<sup>1</sup>*Center for Quantum Devices, Niels Bohr Institute,  
University of Copenhagen, Universitetsparken 5, 2100 Copenhagen, Denmark*

<sup>2</sup>*Department of Condensed Matter Physics, Weizmann Institute of Science, Rehovot, Israel 76100*

<sup>3</sup>*Department of Physics and Astronomy, and Birck Nanotechnology Center,  
Purdue University, West Lafayette, Indiana 47907 USA*

<sup>4</sup>*School of Materials Engineering, and School of Electrical and Computer Engineering,  
Purdue University, West Lafayette, Indiana 47907 USA*

(Dated: January 23, 2023)

We report simultaneously acquired local and nonlocal transport spectroscopy in a phase-biased planar Josephson junction based on an epitaxial InAs/Al hybrid two-dimensional heterostructure. Quantum point contacts at the junction ends allow measurement of the  $2 \times 2$  matrix of local and nonlocal tunneling conductances as a function of magnetic field along the junction, phase difference across the junction, and carrier density. A closing and reopening of a gap was observed in both the local and nonlocal tunneling spectra as a function of magnetic field. For particular tunings of junction density, gap reopenings were accompanied by zero-bias conductance peaks (ZBCPs) in local conductances. End-to-end correlation of gap reopening was strong, while correlation of local ZBCPs was weak. A model of the device, with disorder treated phenomenologically, shows comparable conductance matrix behavior associated with a topological phase transition. Phase dependence helps distinguish possible origins of the ZBCPs.

Topological materials obey a bulk-boundary correspondence, establishing a connection between the topological index of the bulk and the number of boundary modes [1, 2]. In one-dimensional topological superconductors (1D-TSCs) [3, 4], these considerations imply that the bulk modes undergo a characteristic closing and reopening of the superconducting gap whenever the system is driven through a topological phase transition. In this situation, the gap reopening is connected to the appearance of zero-energy Majorana modes at the two ends [5–8]. Several experimental works have reported zero-bias conductance peaks (ZBCPs) at the ends of wires or 1D structures, identified as signatures of 1D-TSCs [9–15]. However, in most of these cases, though not all [16, 17], an associated gap closing and reopening was not observed in tunneling conductance.

An emerging method that allows simultaneous observation of end modes and bulk gap behavior is nonlocal spectroscopy, where measurement of the tunneling current between the ends of a device provides information about the bulk [18], and forms the basis for the identification and measurement of a topological gap [19]. This technique requires a three-terminal (3T) configuration [20–24], and has been theoretically explored in the context of topological superconductivity for nanowires [18, 25–28]. Nonlocal transport experiments, also in nanowires, were used to probe symmetries of the conductance matrix arising from current conservation and measure the local charge of Andreev bound states [26, 29]. Experiments in short nanowire segments identified end-to-end correlation between extended Andreev bound states [30]. In long nanowire segments, local conductance showed ZBCPs while the gap in the

nonlocal spectrum remained closed [31], suggesting non-topological ZBCPs arising from strong disorder [32–36]. These experiments demonstrated the importance of combining local and nonlocal transport to differentiate trivial and potentially topological ZBCPs.

Planar Josephson junctions (PJJs) of superconductor-semiconductor hybrids have recently emerged as a promising alternative platform for topological superconductivity, providing several knobs that can control a possible topological superconducting phase, including, notably, the novel control parameter of the phase difference across the junction [15, 38–44]. However an experimental investigation of nonlocal conductance on this platform is lacking. Challenges associated with the construction of a three-terminal phase-biased SNS junction, together with the small amplitude of the nonlocal conductance signal ( $\sim 0.01 \times 2e^2/h$ ) makes this a significantly harder experiment compared to previous local conductance studies.

In this Letter, we overcome these challenges and investigate nonlocal conductance spectroscopy, measured simultaneously with local conductance spectroscopy in 3T PJJ devices with quantum point contacts (QPCs) at both ends. The full conductance matrix is measured as a function of in-plane magnetic field along the junction, phase difference across the junction, and carrier density within the junction. Our main observation is a closing and reopening of the superconducting gap in *nonlocal* conductance correlated with the appearance of ZBCPs in *local* conductance. This goes beyond previous studies where only local conductance measurements were reported [15, 17, 41–43]. We find that the gap closing and reopening in both local and nonlocal conductance is robust against variations of the junction carrier density,

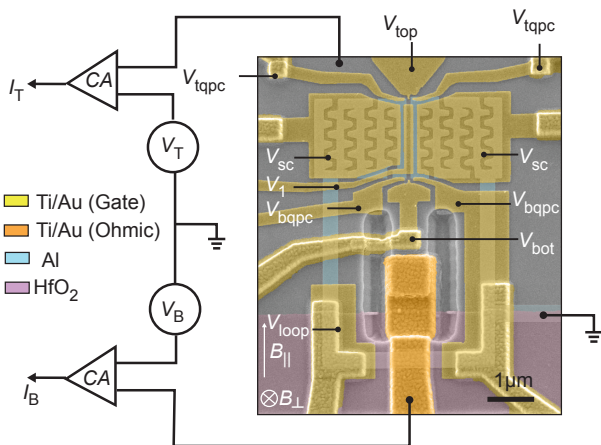


FIG. 1. **Device and measurement setup.** False-color micrograph of a representative device showing three-terminal configuration. Meandering perforations etched onto the superconducting leads allow partial depletion of the semiconductor using gate voltage  $V_{sc}$ . Al loop allows phase biasing of the junction with a small out-of-plane magnetic field,  $B_{\perp}$ . An in-plane magnetic field,  $B_{\parallel}$  is applied parallel to the S-N interfaces. Voltage biases  $V_T$  and  $V_B$  are applied to the top and bottom ohmic contacts through the current amplifiers (CA). Gates  $V_{top(bot)}$  and  $V_{t(b)qpc}$  form QPCs at the junction ends.  $V_1$  controls carrier density in the junction. All connections to the device are via  $\sim 1 - 2$  k $\Omega$  fridge wires and filters, see Supplemental Material for details [37].

but the observation of ZBCPs at one or both ends require careful tuning of voltages on the junction and QPC gates.

To help interpret these results, we investigate numerically the conductance matrix behavior of a planar JJ model reported in our previous work [17] including the effect of disorder. Within the model, a gap reopening in nonlocal conductance appears together with ZBCPs in local conductances only in the cases of weak-intermediate disorder strengths and is associated with a topological phase transition. At large disorder strengths, a topological phase transition fails to occur and is characterized by the absence of a nonlocal gap-reopening, while ZBCPs still appear in local conductances.

Figure 1 shows a micrograph of one of the devices, along with a schematic electrical circuit. The PJJ can be probed by a pair of integrated QPCs at the ends of the junction, and phase-biased by applying a small ( $\sim 0.1$  mT scale) out-of-plane magnetic field through a superconducting loop.

The device was fabricated on a molecular-beam-epitaxy grown heterostructure stack with a shallow InAs quantum well separated from a top Al layer by an  $\text{In}_{0.75}\text{Ga}_{0.25}\text{As}$  barrier. A combination of wet etching of the Al layer and deep wet etching of the semiconductor stack was used to define the superconducting loop, the Josephson junction and the mesa with a U-shaped trench.

A patch of the mesa (with Al removed) within the loop was contacted by a layer of Ti/Au to form an internal submicron ohmic contact to enable bottom-end tunneling spectroscopy. A layer of  $\text{HfO}_2$ , grown by atomic layer deposition (ALD) and patterned in a rectangular shape, was used to isolate the Ti/Au layer from the superconducting loop and the conducting mesa. A second layer of  $\text{HfO}_2$  was deposited globally followed by the deposition of Ti/Au gates for electrostatic control of the junction and the QPCs.

The carrier density in the normal barrier of the JJ (width  $w_n = 100$  nm, length  $l = 1.6$   $\mu\text{m}$ ) was controlled by gate voltage  $V_1$ . Gate voltage  $V_{sc}$  controlled the carrier density in the semiconductor underneath the superconducting leads. Split gates controlled by voltages  $V_{tqpc}$  and  $V_{bqpc}$  define QPCs at the top and bottom of the junction. Additional gate voltages  $V_{top}$  and  $V_{bot}$  controlled densities in the normal regions outside the QPCs, and were typically fixed at  $\sim +100$  mV. Hall effect measurements performed in Hall bar devices of the same material, with Al etched away, indicated a peak electron mobility  $\mu = 43,000$   $\text{cm}^2/\text{V}\cdot\text{s}$  at a carrier density of  $n = 8 \times 10^{11}$   $\text{cm}^{-2}$ , corresponding to a peak electron mean free path of  $l_e \sim 600$  nm. This suggests that our devices are quasiballistic along the length  $l \sim 3l_e$  and ballistic in the width direction  $w_n \sim l_e/6$ . We estimate the Fermi wavelength as  $\lambda_F \simeq 30$  nm, giving  $w_n/\lambda_F \sim 3$  and  $l/\lambda_F \sim 50$ , such that the junction may be treated as quasi-one-dimensional. Other transport properties of similar hybrid planar Josephson junction devices have been reported in previous works [45–48]. We specifically highlight the near unity S-N interface transparencies reported in [46, 48].

The 3T measurement configuration is shown in Fig. 1(a). The top ohmic contact is a region of InAs separated from the junction by the top QPC. The bottom ohmic contact is formed by a Ti/Au electrode, separated by the bottom QPC. The Al loop connecting the two sides of the junction provides the third contact, held at ground. Low-frequency AC plus DC voltage biases  $V_{T(B)}$  are applied through current amplifiers (denoted CA). The measured currents  $I_{T(B)}$  then yield the  $2 \times 2$  conductance matrix,  $G_{ij} = dI_i/dV_j$ , with  $i, j = T, B$  via standard AC lock-in measurements (see additional details in Supplemental Material [37]).

For measurements shown in Fig. 2, the conductance matrix was measured as a function of in-plane magnetic field,  $B_{\parallel}$ , with  $V_{sc} = -3.6$  V, giving a hard superconducting gap in the leads,  $V_1 = +85$  mV, giving ZBCPs in both top and bottom local conductances at  $B_{\parallel} \sim 0.3$  T, and QPCs set to  $V_{tqpc} = -0.37$  V,  $V_{bqpc} = -0.34$  V, to yield sizable nonlocal conductances,  $\sim 0.01 \times 2e^2/h$  near the gap edge,  $|V_{T,B}| \sim 150$   $\mu\text{V}$ . To compensate any coupling of  $B_{\parallel}$  through the superconducting loop controlling phase  $\Phi$  across the junction, a sweep of  $B_{\perp}$  was made at each value of  $B_{\parallel}$  and then sliced along cuts of constant  $\Phi$

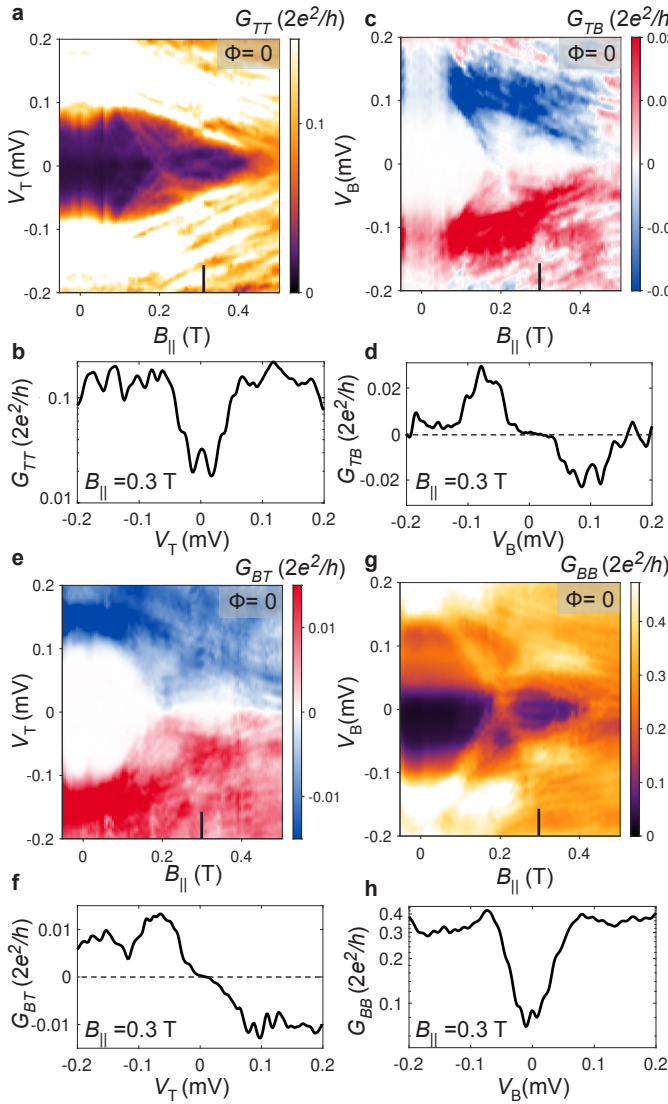


**FIG. 2. Magnetic field dependence of the conductance matrix.** (a) Local differential conductance  $G_{TT}$  and (e) Non-local differential conductance  $G_{BT}$  measured as a function of  $V_T$  and  $B_{\parallel}$ . (c) Nonlocal differential conductance  $G_{TB}$  and (g) local differential conductance  $G_{BB}$  measured as a function of  $V_B$  and  $B_{\parallel}$ . The phase bias is set to  $\Phi = 0$ . Line-cuts at  $B_{\parallel} = 0.3$  T where (b)  $G_{TT}$  shows a ZBCP. (h)  $G_{BB}$  shows a ZBCP. (d)  $G_{TB}$  and (f)  $G_{BT}$  are strongly antisymmetric at high DC biases, and zero in a finite range around zero DC bias. Gate voltage settings used for this measurement were  $V_{tqpc} = -0.37$  V,  $V_{bqpc} = -0.34$  V,  $V_1 = 0.085$  V and  $V_{sc} = -3.6$  V.

numerically by following  $\Phi$ -dependent lobe features (see Methods). This allowed us to obtain the  $B_{\parallel}$  dependence of the conductance matrix at fixed flux, as shown, for instance, in Fig. 2 for  $\Phi = 0$ .

Local conductance spectra showed a finite superconducting gap around  $B_{\parallel} = 0$  [Fig. 2(a, g)]. With increasing  $B_{\parallel}$ , a band of resolvable discrete states moved to-

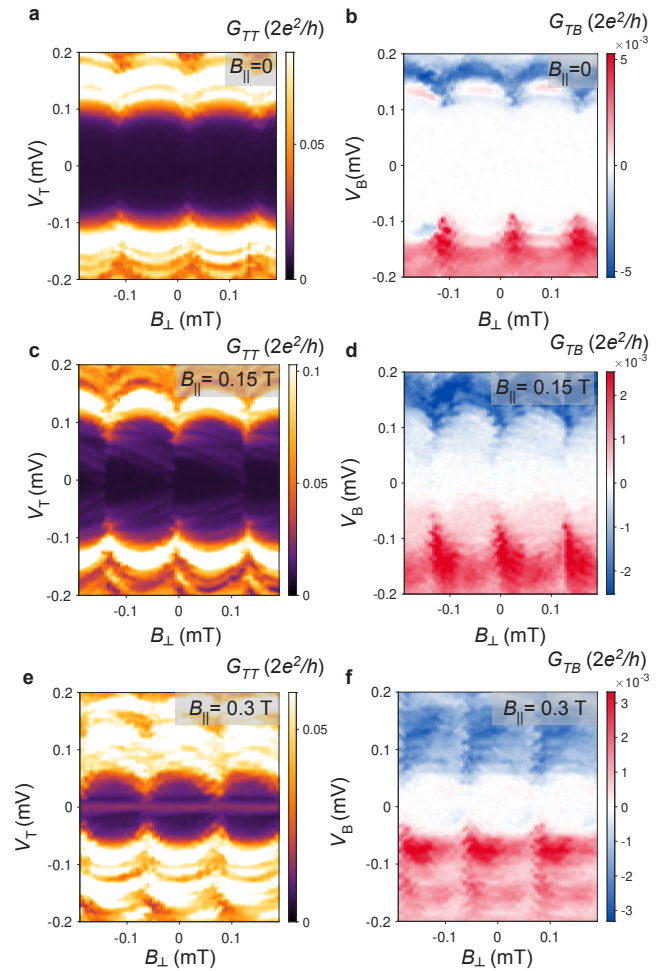


**FIG. 3. Phase dependence of local and nonlocal conductance spectra.** Local differential conductance  $G_{TT}$  (left column) and nonlocal differential conductance  $G_{TB}$  (right column) measured as a function of out-of-plane magnetic field  $B_{\perp}$  and source-drain bias,  $V_T$  and  $V_B$ , respectively at three values of the in-plane magnetic field. (a) and (b)  $B_{\parallel} = 0$ , showing a periodic modulation of the superconducting gap in both the local and nonlocal spectrum. The nonlocal spectrum shows a larger amplitude of the superconducting gap than the local conductance spectrum. (c) and (d)  $B_{\parallel} = 0.15$  T, shows sub-gap states that are lowered in energy. These states are phase-asymmetric and appear in both  $G_{TT}$  and  $G_{TB}$ . (e) and (f)  $B_{\parallel} = 0.3$  T shows a phase-independent ZBCP in  $G_{BB}$ , but not in  $G_{TB}$ .  $G_{TB}$  displays a superconducting gap that is modulated periodically with  $B_{\perp}$ . Gate voltage settings used for this measurement were  $V_{tqpc} = -0.385$  V,  $V_{bqpc} = -0.38$  V,  $V_1 = 0.092$  V and  $V_{sc} = -3.6$  V.

wards zero bias, closing the gap at  $B_{\parallel} \sim 0.2$  T followed by its reopening. Beyond the reopening ( $0.2$  T  $< B_{\parallel} < 0.4$  T), but not before, ZBCPs were observed in both  $G_{TT}$  and  $G_{BB}$  [Fig. 2(b, h)]. In this data set, the ZBCP at the top end splits as  $B_{\parallel}$  approaches 0.4 T, whereas the bottom end ZBCP appears to remain at zero, but diminishes in amplitude. Additionally, the ZBCPs observed at



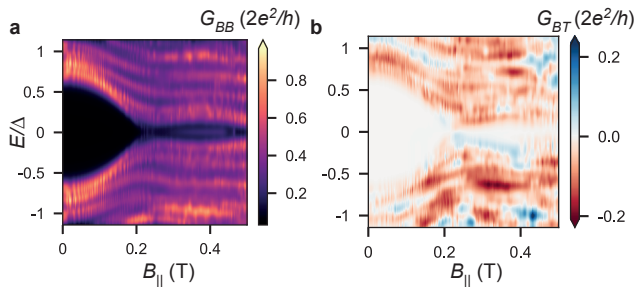


FIG. 4. **Numerical simulation of local and nonlocal conductance.** (a) Local conductance  $G_{BB}$  evaluated at the bottom end of the junction as a function of  $B_{\parallel}$ , and  $\Phi = 0$  including thermal broadening equivalent to a temperature of 50 mK. At  $B_{\parallel} \sim 0.2$  T the junction undergoes a topological phase transition reflected by the closing and reopening of the superconducting gap, followed by the appearance of a ZBCP. (b) Nonlocal conductance  $G_{BT}$  shows a corresponding gap-reopening transition at  $B_{\parallel} \sim 0.2$  T without the formation of a ZBCP.

each end do not exhibit strong correlation with respect to variations of  $V_1$  (see Fig. S10). Both local conductances show a final gap closure at  $B_{\parallel} \sim 0.45$  T.

The corresponding behavior of the nonlocal conductance spectra is shown in Figs. 2(c, e). A predominantly antisymmetric signal is observed throughout the measured magnetic field range, with amplitude remaining roughly uniform. The gap in the nonlocal spectrum undergoes a closure at  $B_{\parallel} \sim 0.2$  T, at the same magnetic field as the local conductance spectrum, and is visible in both  $G_{TB}$  and  $G_{BT}$ . Both nonlocal conductances remain strongly antisymmetric around zero bias. The nonlocal gap then reopens obtaining a maximum at  $B_{\parallel} \sim 0.3$  T, with line-cuts shown in Figs. 2(d, f). Notably, no ZBCP is observed. Both nonlocal conductances disappear in a finite window around zero bias before turning on sharply at finite  $V_{T/B}$ . The final closure of the nonlocal gap at  $B_{\parallel} \sim 0.45$  T is more pronounced, in terms of signal strength, than the closure at  $B_{\parallel} \sim 0.2$  T.

Local and nonlocal conductance spectra are modulated by a small perpendicular magnetic field,  $B_{\perp}$ , which threads flux through the  $\sim 12 \mu\text{m}^2$  superconducting loop ( $B_{\perp} \sim 0.17$  mT corresponds to  $\Phi_0 = h/2e$  through the loop), showing the same period in  $B_{\perp}$  and in phase. Around  $B_{\parallel} = 0$  [Figs. 3(a, b)], the local gap in  $G_{TT}$  appears smaller than the nonlocal gap in  $G_{BT}$ . At  $B_{\parallel} \sim 0.15$  T [Figs. 3(c),(d)], flux-dependent states are lowered in energy and fill the sub-gap spectrum in both local and nonlocal conductances. Within each flux lobe, states are asymmetric with respect to  $\Phi$ . At  $B_{\parallel} = 0.3$  T, a phase-independent ZBCP is measured in  $G_{TT}$  [Fig. 3(e)] but absent in  $G_{BT}$  [Fig. 3(f)]. At this field,  $G_{BT}$  remains zero until a source-drain bias of  $V_T \sim 40 \mu\text{eV}$  at  $\Phi = 0$  and closes at  $\Phi = \Phi_0/2$ .  $G_{TB}$  and  $G_{BB}$ , are qualitatively similar to  $G_{BT}$  and  $G_{TT}$  respectively (see Fig. S9).

We also investigated nonlocal transport at gate settings where a ZBCP was observed in the bottom local conductance, but not the top local conductance (see Fig. S4 and S5). In this case, a gap-reopening signature was observed in nonlocal conductance and the nonlocal gap remained finite in the reopened state. In other devices where reasonably strong nonlocal conductance was observed ( $\sim 0.01 \times 2e^2/h$ ), the nonlocal spectrum exhibited a gap-reopening feature. In some cases, the sub-gap nonlocal conductance in the reopened state remained finite, indicating a soft nonlocal gap (see Figs. S11 and S12, [37]). Typically, we observed that ZBCPs appeared at one or both ends of the device with more probability at positive settings of the gate voltage  $V_1 \sim 0 - 200$  mV. This may be attributed to strong screening of charge impurities due to larger channel carrier densities at these voltage settings. Voltages larger than  $V_1 \simeq 200$  mV could not be applied due to gate leakage. A systematic study of this effect is left for future work.

To help interpret characteristic features of the observed conductance matrix, we investigate a model of a PJJ using the Kwant software package [49], as described previously [17]. Here, we extend the model by tunnel coupling the system to metallic leads at the junction ends. We first investigate the disorder-free case with results shown in Fig. 4. Top-bottom symmetry of the model ensures that  $G_{TT} = G_{BB}$  and  $G_{TB} = G_{BT}$ . Figure 4(a) shows the local conductance spectrum undergoing a topological gap-reopening transition at  $B_{\parallel} \sim 0.2$  T, followed by a ZBCP arising from a Majorana zero mode. The corresponding nonlocal conductance spectrum, shown in Fig. 4(b), also shows a reopening of the gap, but no sub-gap structure once the gap reopens.

We note that the phase difference  $\phi$  does not have a strong influence on the critical magnetic field  $B_c \simeq 0.2$  T required for gap-closing and reopening. This is unlike the predictions of models reported in [38, 39] where  $B_c$  is strongly modulated by  $\phi$  and can reach zero in a perfectly transparent junction when  $\phi \sim \pi$ . Reduced phase-modulation is expected in our model due to the orbital effect from the in-plane magnetic field, as shown in  $B_{\parallel} - \phi$  phase diagrams comparing the two models (see Fig. S17). Experimental limitations arising from the finite inductance of the phase biasing loop ( $\sim 2$  nH, see [17]) and normal backscattering at the S-N interfaces [39] may further reduce the effect of  $\phi$ .

These model results support the interpretation that nonlocal conductance is mediated by a combination of co-tunneling and crossed-Andreev reflection of quasiparticles carried by extended Andreev bound states. These states have a finite probability density throughout the length of the junction, including the two ends, and therefore also appear in the local conductances. Within this picture, Majorana zero-modes appear as zero-bias peaks only in local conductance, not in nonlocal conductance because of their localized probability density. This is in

contrast to extended Andreev bound states, which are expected to appear in both local and nonlocal conductances [27, 29].

Including disorder within the model, we find that conductance matrix signatures are qualitatively similar to the disorder-free case as long as the disorder strength is limited within a weak-to-intermediate regime (see Figs. S13 and S14, [37]). All these regimes show a non-local gap reopening with ZBCPs in local conductances, associated with a topological phase. On the other hand, strong disorder destroys topology and produces a characteristic closed-gap signature in nonlocal spectroscopy (see Fig. S15). Non-topological ZBCPs are still possible in local conductances.

Conductance matrix signatures obtained from our model for the cases of weak-to-intermediate disorder are consistent with experiment. However, as opposed to the experiment, in the numerical simulations we find a large symmetric component of the nonlocal conductance, comparable in strength to the antisymmetric component. Their relative strength depends on details used to model finite temperature, disorder, and tunneling barriers [18, 28], and may explain this discrepancy. Finally, local ZBCPs are fully correlated in the model, but lack such correlation in experiment.

Within a non-topological interpretation of our data, an inhomogeneous chemical potential profile produces non-topological zero-energy Andreev bound states at the two device ends. In the model these states are not stable at zero-energy with respect to variation of  $\Phi$ , which may provide a distinguishing signature. Another non-topological scenario is the case of strong disorder, where a proliferation of low-energy sub-gap states prevents a topological phase transition. This scenario can produce ZBCPs in local conductance, but does not show a gap-reopening in the nonlocal conductance as discussed in Fig. S15, and consistent with previous nanowire results [25, 31].

Within a topological interpretation, the presence of a finite nonlocal gap without strong end-to-end ZBCP correlation may arise from charge impurity disorder [50]. In the case of nanowires, it was shown that a low density  $\sim 10^{15}/\text{cm}^3$  of charge impurities may create disjointed topological segments and reduce or even eliminate end-to-end ZBCP correlation, while still preserving topology. We speculate that similar physics is possible in planar JJs, but our present model cannot capture this effect. In addition, various sources of disorder including interface and bulk charged impurities, surface roughness and edge roughness at the S-N interfaces are likely to be important and their effects on the topological phase in planar JJs remains to be investigated. Theoretical studies of conductance matrix behavior including such disorder effects may be directly compared against our experimental data to help further clarify the situation.

We thank Geoff Gardner and Sergei Gronin for con-

tributions to materials growth, and Asbjørn Drachmann for assistance with fabrication. We thank Lucas Casparis, Tom Dvir, Karsten Flensberg, Max Geier, Esteban Martinez, and Andreas Pöschl, for valuable discussions. We acknowledge a research grant (Project 43951) from VILLUM FONDEN, support from the ERC under the Horizon 2020 Research and Innovation programme (LEGOTOP No. 788715 and HQMAT No. 817799), the DFG (CRC/Transregio 183, EI 519/7-1), the BSF and NSF (2018643), the ISF Quantum Science and Technology (2074/19), and a research grant from Irving and Cherna Moskowitz.

- 
- [1] X.-L. Qi and S.-C. Zhang, *Rev. Mod. Phys.* **83**, 1057 (2011).
  - [2] L. Fu and C. L. Kane, *Phys. Rev. Lett.* **100**, 096407 (2008).
  - [3] Y. Oreg, G. Refael, and F. von Oppen, *Phys. Rev. Lett.* **105**, 177002 (2010).
  - [4] R. M. Lutchyn, J. D. Sau, and S. Das Sarma, *Phys. Rev. Lett.* **105**, 077001 (2010).
  - [5] J. D. Sau, S. Tewari, R. M. Lutchyn, T. D. Stanescu, and S. Das Sarma, *Phys. Rev. B* **82**, 214509 (2010).
  - [6] T. D. Stanescu, R. M. Lutchyn, and S. Das Sarma, *Phys. Rev. B* **84**, 144522 (2011).
  - [7] S. Tewari, J. D. Sau, V. W. Scarola, C. Zhang, and S. Das Sarma, *Phys. Rev. B* **85**, 155302 (2012).
  - [8] D. Rainis, L. Trifunovic, J. Klinovaja, and D. Loss, *Phys. Rev. B* **87**, 024515 (2013).
  - [9] V. Mourik, K. Zuo, S. M. Frolov, S. R. Plissard, E. P. A. M. Bakkers, and L. P. Kouwenhoven, *Science* **336**, 1003 (2012).
  - [10] S. Nadj-Perge, I. K. Drozdov, J. Li, H. Chen, S. Jeon, J. Seo, A. H. MacDonald, B. A. Bernevig, and A. Yazdani, *Science* **346**, 602 (2014).
  - [11] A. Das, Y. Ronen, Y. Most, Y. Oreg, M. Heiblum, and H. Shtrikman, *Nature Physics* **8**, 887 (2012).
  - [12] M. Deng, S. Vaitiekėnas, E. B. Hansen, J. Danon, M. Leijnse, K. Flensberg, J. Nygård, P. Krogstrup, and C. M. Marcus, *Science* **354**, 1557 (2016).
  - [13] F. Nichele, A. C. C. Drachmann, A. M. Whiticar, E. C. T. O'Farrell, H. J. Suominen, A. Fornieri, T. Wang, G. C. Gardner, C. Thomas, A. T. Hatke, P. Krogstrup, M. J. Manfra, K. Flensberg, and C. M. Marcus, *Phys. Rev. Lett.* **119**, 136803 (2017).
  - [14] A. Grivnin, E. Bor, M. Heiblum, Y. Oreg, and H. Shtrikman, *Nature Comm.* **10**, 1 (2019).
  - [15] A. Fornieri, A. M. Whiticar, F. Setiawan, E. Portolés, A. C. Drachmann, A. Keselman, S. Gronin, C. Thomas, T. Wang, R. Kallaher, *et al.*, *Nature* **569**, 89 (2019).
  - [16] S. Vaitiekėnas, M.-T. Deng, J. Nygård, P. Krogstrup, and C. M. Marcus, *Phys. Rev. Lett.* **121**, 037703 (2018).
  - [17] A. Banerjee, O. Lesser, M. A. Rahman, H.-R. Wang, M.-R. Lee, A. Kringhøj, A. M. Whiticar, A. C. C. Drachmann, C. Thomas, T. Wang, G. C. Gardner, M. J. Manfra, E. Berg, Y. Oreg, A. Stern, and C. M. Marcus, *ArXiv* 2201.03453 (2022).
  - [18] T. O. Rosdahl, A. Vuik, M. Kjaergaard, and A. R. Akhmerov, *Phys. Rev. B* **97**, 045421 (2018).

- [19] D. I. Pikulin, B. van Heck, T. Karzig, E. A. Martinez, B. Nijholt, T. Laeven, G. W. Winkler, J. D. Watson, S. Heedt, M. Temurhan, *et al.*, arXiv preprint arXiv:2103.12217 (2021).
- [20] L. Hofstetter, S. Csonka, J. Nygård, and C. Schönberger, *Nature* **461**, 960 (2009).
- [21] L. G. Herrmann, F. Portier, P. Roche, A. L. Yeyati, T. Kontos, and C. Strunk, *Phys. Rev. Lett.* **104**, 026801 (2010).
- [22] J. Schindele, A. Baumgartner, and C. Schönberger, *Physical review letters* **109**, 157002 (2012).
- [23] J. Schindele, A. Baumgartner, R. Maurand, M. Weiss, and C. Schönberger, *Physical Review B* **89**, 045422 (2014).
- [24] J. Gramich, A. Baumgartner, and C. Schönberger, *Physical Review B* **96**, 195418 (2017).
- [25] H. Pan, J. D. Sau, and S. Das Sarma, *Phys. Rev. B* **103**, 014513 (2021).
- [26] J. Danon, A. B. Hellenes, E. B. Hansen, L. Casparis, A. P. Higginbotham, and K. Flensberg, *Phys. Rev. Lett.* **124**, 036801 (2020).
- [27] R. Hess, H. F. Legg, D. Loss, and J. Klinovaja, *Phys. Rev. B* **104**, 075405 (2021).
- [28] G. Wang, T. Dvir, N. van Loo, G. P. Mazur, S. Gazibegovic, G. Badawy, E. P. Bakkers, L. P. Kouwenhoven, and G. de Lange, arXiv preprint arXiv:2110.05373 (2021).
- [29] G. C. Ménard, G. L. R. Anselmetti, E. A. Martinez, D. Puglia, F. K. Malinowski, J. S. Lee, S. Choi, M. Pendharkar, C. J. Palmstrøm, K. Flensberg, C. M. Marcus, L. Casparis, and A. P. Higginbotham, *Phys. Rev. Lett.* **124**, 036802 (2020).
- [30] G. L. R. Anselmetti, E. A. Martinez, G. C. Ménard, D. Puglia, F. K. Malinowski, J. S. Lee, S. Choi, M. Pendharkar, C. J. Palmstrøm, C. M. Marcus, L. Casparis, and A. P. Higginbotham, *Phys. Rev. B* **100**, 205412 (2019).
- [31] D. Puglia, E. A. Martinez, G. C. Ménard, A. Pöschl, S. Gronin, G. C. Gardner, R. Kallagher, M. J. Manfra, C. M. Marcus, A. P. Higginbotham, and L. Casparis, *Phys. Rev. B* **103**, 235201 (2021).
- [32] D. Bagrets and A. Altland, *Phys. Rev. Lett.* **109**, 227005 (2012).
- [33] E. Prada, P. San-Jose, and R. Aguado, *Phys. Rev. B* **86**, 180503 (2012).
- [34] C.-X. Liu, J. D. Sau, T. D. Stanescu, and S. Das Sarma, *Phys. Rev. B* **96**, 075161 (2017).
- [35] H. Pan, W. S. Cole, J. D. Sau, and S. Das Sarma, *Phys. Rev. B* **101**, 024506 (2020).
- [36] H. Pan and S. Das Sarma, *Phys. Rev. Research* **2**, 013377 (2020).
- [37] See Supplemental Material [URL](#) which includes Refs. 51-54.
- [38] M. Hell, M. Leijnse, and K. Flensberg, *Phys. Rev. Lett.* **118**, 107701 (2017).
- [39] F. Pientka, A. Keselman, E. Berg, A. Yacoby, A. Stern, and B. I. Halperin, *Phys. Rev. X* **7**, 021032 (2017).
- [40] F. Setiawan, A. Stern, and E. Berg, *Phys. Rev. B* **99**, 220506 (2019).
- [41] M. C. Dartiailh, W. Mayer, J. Yuan, K. S. Wickramasinghe, A. Matos-Abiague, I. Žutić, and J. Shabani, *Phys. Rev. Lett.* **126**, 036802 (2021).
- [42] H. Ren, F. Pientka, S. Hart, A. T. Pierce, M. Kosowsky, L. Lunczer, R. Schlereth, B. Scharf, E. M. Hankiewicz, L. W. Molenkamp, *et al.*, *Nature* **569**, 93 (2019).
- [43] C. T. Ke, C. M. Moehle, F. K. de Vries, C. Thomas, S. Metti, C. R. Guinn, R. Kallagher, M. Lodari, G. Scappucci, T. Wang, *et al.*, *Nature Comm.* **10**, 1 (2019).
- [44] D. Z. Haxell, E. Cheah, F. Křížek, R. Schott, M. F. Ritter, M. Hinderling, W. Belzig, C. Bruder, W. Wegscheider, H. Riel, and F. Nichele, arXiv (2022), [2204.05619](#).
- [45] J. Shabani, M. Kjaergaard, H. J. Suominen, Y. Kim, F. Nichele, K. Pakrouski, T. Stankevic, R. M. Lutchyn, P. Krogstrup, R. Feidenhans'l, S. Kraemer, C. Nayak, M. Troyer, C. M. Marcus, and C. J. Palmstrøm, *Phys. Rev. B* **93**, 155402 (2016).
- [46] M. Kjaergaard, H. J. Suominen, M. P. Nowak, A. R. Akhmerov, J. Shabani, C. J. Palmstrøm, F. Nichele, and C. M. Marcus, *Phys. Rev. Applied* **7**, 034029 (2017).
- [47] H. J. Suominen, J. Danon, M. Kjaergaard, K. Flensberg, J. Shabani, C. J. Palmstrøm, F. Nichele, and C. M. Marcus, *Phys. Rev. B* **95**, 035307 (2017).
- [48] F. Nichele, E. Portolés, A. Fornieri, A. M. Whiticar, A. C. C. Drachmann, S. Gronin, T. Wang, G. C. Gardner, C. Thomas, A. T. Hatke, M. J. Manfra, and C. M. Marcus, *Phys. Rev. Lett.* **124**, 226801 (2020).
- [49] C. W. Groth, M. Wimmer, A. R. Akhmerov, and X. Waintal, *New Journal of Physics* **16**, 063065 (2014).
- [50] B. D. Woods, S. Das Sarma, and T. D. Stanescu, *Phys. Rev. Applied* **16**, 054053 (2021).
- [51] E. A. Martinez, A. Pöschl, E. B. Hansen, M. A. Y. van de Poll, S. Vaitiekėnas, A. P. Higginbotham, and L. Casparis, arXiv:2104.02671 (2021).
- [52] R. Peierls, *Zeitschrift für Physik* **80**, 763 (1933).
- [53] M. Tinkham, *Introduction to Superconductivity*, 2nd ed., International Series in Pure and Applied Physics (McGraw-Hill, New York, 1996).
- [54] S. Ahn, H. Pan, B. Woods, T. D. Stanescu, and S. Das Sarma, *Phys. Rev. Materials* **5**, 124602 (2021).